

Unconventional superconductivity in a non-centrosymmetric α -Mn alloy NbTaOs₂

R. K. Kushwaha ¹, Arushi ¹, S. Jangid,¹ P. K. Meena,¹ R. Stewart,² A. D. Hillier ² and R. P. Singh ^{1,*}

¹*Department of Physics, Indian Institute of Science Education and Research Bhopal, Bhopal, 462066, India*

²*ISIS Facility, STFC Rutherford Appleton Laboratory, Harwell Science and Innovation Campus, Oxfordshire, OX11 0QX, UK*

Non-centrosymmetric superconductors have emerged as a fascinating avenue for exploring unconventional superconductivity. Their broken inversion and time-reversal symmetries make them prime candidates for realizing the intrinsic superconducting diode effect (SDE). In this work, we synthesize the ternary non-centrosymmetric α -Mn alloy NbTaOs₂ and conduct a comprehensive investigation of its superconducting properties through resistivity, magnetization, specific heat and muon spin rotation/relaxation (μ SR) techniques. Our transverse field- μ SR and specific heat results provide evidence of a moderately coupled, fully-gapped superconducting state. Zero field- μ SR measurements reveal a subtle increase in the relaxation rate below the transition temperature, suggesting time reversal symmetry breaking in the superconducting ground state of NbTaOs₂.

I. INTRODUCTION

The superconducting order parameter, defined by complex gap functions, reveals the macroscopic quantum state, with its symmetry crucial for superconductor classification. While conventional superconductors break only gauge symmetry U(1), unconventional superconductors can disrupt additional symmetries, including time-reversal, rotational, and inversion symmetries [1]. Non-centrosymmetric superconductors (NCSs), lacking inversion symmetry, represent a distinct class of unconventional superconductors [2, 3]. The resulting antisymmetric spin-orbit coupling (ASOC) in these materials enables mixing of the spin-singlet and spin-triplet pairing states [3, 4]. This mixed pairing leads to unique phenomena in NCSs, such as nodes/nodal lines and multigap behavior [5–7], an upper critical field exceeding the Pauli limit [8], and non-trivial topological states [9–11].

Recent studies predict that NCSs exhibit a range of unique effects, including piezosuperconductivity [12], chiral superconductivity [13], field-reversed vortices [14], nonlinear responses [15, 16], and a superconducting analog of the Chandrasekhar-Kendall state [17]. Notably, NCSs emerge as ideal materials in which to realize the intrinsic superconducting diode effect (SDE) [18, 19]. Their inherently broken inversion and time-reversal symmetries provide a natural and simplified pathway to achieve SDE, in contrast to conventional approaches that rely on complex heterostructures and externally applied magnetic fields [20, 21].

While NCSs exhibiting time-reversal symmetry breaking (TRSB) are theoretically intriguing, they remain experimentally rare, highlighting the need for further discovery and characterization. TRSB in the superconducting state [22] has been observed across various centrosymmetric (CS) and non-centrosymmetric (NC) crystal structures [11, 23–36]. Notably, rhenium-based NCSs

with the α -Mn structure reported a frequent occurrence of TRSB with fully gapped superconductivity [29–31]. The critical percentage of rhenium in these compounds, along with the complex interplay of the crystal structure and ASOC, is believed to be critical for TRSB. This is further evidenced by the lack of TRSB in non-rhenium-based superconductors [37–39]. However, most of the work on NCS is focused on binary compounds, and TRSB is not universal in α -Mn structured superconductors [37–42]. This suggests that other factors are at play in determining TRSB presence or absence in NCSs, highlighting the need to discover and characterize new noncentrosymmetric superconductors.

We have synthesized a new ternary compound NbTaOs₂, which crystallizes in the non-centrosymmetric α -Mn structure and is known for its intrinsic disorder. Due to the mixing of 4d niobium and 5d tantalum atoms on the atomic sites, we expect enhanced ASOC and further disorder. This will help to understand the complex interplay of crystal structure, ASOC, and the effect of disorder on the superconducting ground state. Furthermore, this study may provide insight into the role of the critical percentage of a specific element in determining the presence and absence of TRSB in the superconducting ground state [43].

In this paper, we investigate the superconducting properties of NbTaOs₂ using electrical resistivity, magnetization, specific heat, and muon spin rotation/relaxation (μ SR) measurements. Our findings confirm that NbTaOs₂ exhibits bulk type II superconductivity, with a superconducting transition temperature of 2.4(2) K. Both the specific heat and transverse field μ SR measurements confirm an isotropic superconducting gap. Zero-field μ SR measurements show an increased relaxation rate below the superconducting transition temperature, suggesting a broken time-reversal symmetry in the superconducting ground state of NbTaOs₂. This makes NbTaOs₂ the first non-Re-based α -Mn superconducting compound to exhibit time-reversal symmetry breaking.

* rpsingh@iiserb.ac.in

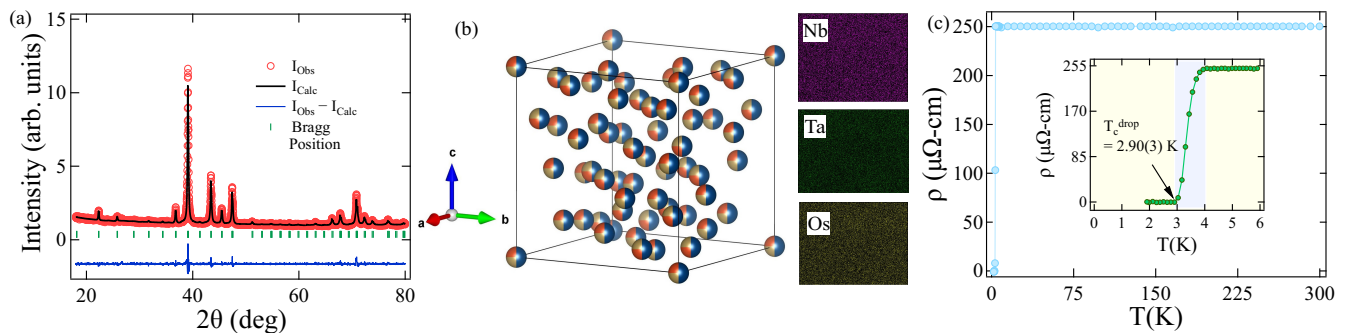


FIG. 1. (a) Powder XRD pattern of NbTaOs₂ obtained at room temperature is indicated by the red circles; while the solid black lines represent the Rietveld refinement. (b) NbTaOs₂ crystal structure (left) and the elemental mapping (right) of Nb, Ta, and Os elements. (c) Temperature-dependent resistivity of NbTaOs₂, inset shows the superconducting transition temperature.

II. EXPERIMENTAL DETAILS

A polycrystalline sample of NbTaOs₂ was synthesized by melting high-purity metals (3N) Nb, Ta, and Os in a stoichiometric ratio in an argon atmosphere. Phase purity and crystal structure were analyzed using powder X-ray diffraction (XRD) with Cu K_α radiation ($\lambda=1.5406$ Å) on a PANalytical powder X-ray diffractometer and the XRD patterns were refined using Fullprof software [44]. Energy dispersive X-ray analysis (EDAX) was performed using an Oxford high-resolution field emission scanning electron microscope (SEM) to determine the elemental composition and obtain spatial elemental mapping. DC and AC susceptibility measurements were performed using a Quantum Design magnetic property measurement system (MPMS3). The electrical resistivity and heat capacity measurements were performed on a Quantum Design Physical Property Measurement System (PPMS). Muon spin rotation/relaxation (μ SR) measurements were performed on the MUSR spectrometer at the ISIS pulsed neutron and muon facility at Rutherford Appleton Laboratory [45].

III. RESULTS

A. Sample Characterization

The room-temperature powder XRD pattern at room temperature of NbTaOs₂ is presented in Fig. 1(a). Rietveld refinement confirms the phase purity, revealing that NbTaOs₂ crystallizes in the cubic structure α -Mn with space group I43m. The refined lattice parameters are $a = b = c = 9.7703(2)$ Å, with a unit cell volume of $V_{cell} = 932.65(7)$ Å³. Fig. 1(b) illustrates the NCS cubic crystal structure (left), where site mixing occurs at each lattice point. Furthermore, EDAX analysis verifies the elemental composition, showing Nb (24%), Ta (24.5%) and Os (51.5%), which aligns closely with the nominal stoichiometric ratio of NbTaOs₂. Figure 1(b) represents the elemental mapping (right).

B. Resistivity

Temperature-dependent electrical resistivity $\rho(T)$ measurements were performed, which confirm the superconducting transition in NbTaOs₂. The zero field $\rho(T)$ did not show a significant change in resistivity from room temperature (300 K) down to 4 K. The residual resistivity ratio (RRR) ~ 1 , suggests intrinsic disorder, which is also observed in other α -Mn binary and ternary compounds [46]. The variation of $\rho(T)$ is shown in Fig. 1 (c), while the inset highlights the emergence of zero resistivity at the transition temperature, $T_c = 2.90(3)$ K. Compared to magnetization and specific heat measurements, the higher T_c observed in resistivity measurements suggests the presence of surface superconductivity [47].

C. Magnetization

Temperature-dependent magnetization measurements were conducted on NbTaOs₂ sample using zero-field cooled warming (ZFCW) and field cooled cooling (FCC) modes [see Fig. 2(a)], confirming the bulk superconductivity with a transition temperature of $T_c = 2.4(2)$ K. Furthermore, measurement of AC susceptibility (inset of Fig. 2(a)) confirms T_c of NbTaOs₂.

Temperature and field-dependent magnetization measurements were performed to determine the superconducting parameters of NbTaOs₂. Using the Ginzburg-Landau (GL) relation (Eq. (1)), the lower critical field, $H_{c1}(0)$, was determined from the measured low field isothermal magnetization curves, where H_{c1} at each temperature was identified as the point where the curves deviate from the Meissner line (solid black line) as shown in the inset of Fig. 2(b).

$$H_{c1}(T) = H_{c1}(0) [1 - (T/T_c)^2] \quad (1)$$

Using Eq. (1) $H_{c1}(0)$ was found to be 2.85(3) mT.

Further, the upper critical field $H_{c2}(0)$ was estimated by measuring the temperature-dependent susceptibility curves at different magnetic fields, and the onset of the diamagnetic signal is considered field-dependent T_c . H_{c2}

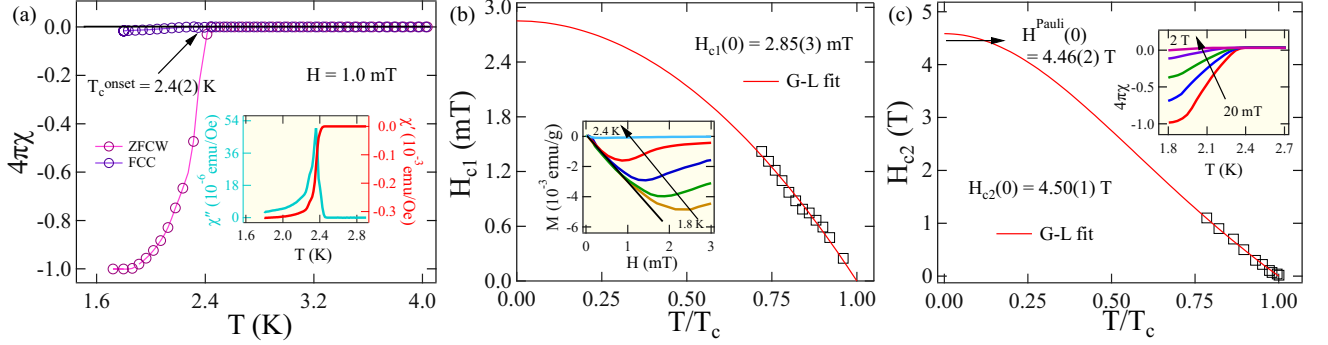


FIG. 2. (a) Temperature *vs.* magnetic susceptibility curves in ZFCW and FCC mode at 1 mT and the inset shows the real and imaginary parts of AC susceptibility. (b) Lower critical field *vs.* reduced temperature (T/T_c) plot, the red curve represents the GL fit using Eq. (1) and the inset shows the field-dependent magnetization at different temperatures. (c) Upper critical field *vs.* T/T_c plot, where the red curve represents GL fit using Eq. (2) and the inset shows the temperature *vs.* susceptibility curves at different fields.

was plotted against temperature, which is well described by the GL relation (Eq. (2)),

$$H_{c2}(T) = H_{c2}(0) \frac{(1 - t^2)}{(1 + t^2)}; \quad \text{where } t = T/T_c \quad (2)$$

The GL fit using Eq. (2) is indicated by the red curve in Fig. 2(c), which yields an estimated value of $H_{c2}(0) = 4.5(1)$ T.

Under an external magnetic field, Cooper pairs can break through two mechanisms: orbital pair breaking and the Pauli limiting field. The orbital limiting field is described by the Werthamer-Helfand-Hohenberg (WHH) [48, 49] model, neglecting the effects of both spin-orbit scattering and Pauli paramagnetism, which is defined as the following equation

$$H_{c2}^{orb}(0) = -\alpha T_c \left. \frac{dH_{c2}(T)}{dT} \right|_{T=T_c} \quad (3)$$

We estimate the initial slope of the upper critical field near the critical temperature, given by, $\left(\frac{-dH_{c2}(T)}{dT}\right)$, to be 0.89 T/K. In dirty limit superconductivity, the orbital limiting field can be approximated using the parameter $\alpha = 0.693$, yielding an estimated value of $H_{c2}^{orb}(0) = 1.5(1)$ T. For conventional BCS superconductors, the Pauli limiting field is given by $H^{Pauli} = 1.86 T_c$ [50, 51]. The estimated H^{Pauli} value is found to be 4.46(2) T by using $T_c = 2.4(2)$ K obtained from magnetization measurements. Interestingly, the estimated upper critical field, $H_{c2}(0) = 4.5(1)$ T, is close to the Pauli pair-breaking limit. This suggests that spin-orbit scattering due to impurities or intrinsic spin-orbit interactions, predicted for non-centrosymmetric superconductors, may be influencing the system, leading to $H_{c2}(0)/H^{Pauli} \geq 1$ [52–54]. To gain insight into characteristic lengths, we employ Ginzburg-Landau (GL) theory to estimate the superconducting coherence length, $\xi_{GL}(0)$ [55] using the expression

$$H_{c2}(0) = \frac{\Phi_0}{2\pi\xi_{GL}^2} \quad (4)$$

where, $\Phi_0 (= 2.07 \times 10^{-15} \text{ T m}^2)$ is the magnetic flux quantum. Substituting $H_{c2}(0) = 4.5(1)$ T, we obtain $\xi_{GL}(0) = 85.4(4)$ Å.

The GL penetration depth, $\lambda_{GL}(0)$ [56], is estimated from the equation Eq. (5)

$$H_{c1}(0) = \frac{\Phi_0}{4\pi\lambda_{GL}^2(0)} \left(\ln \frac{\lambda_{GL}(0)}{\xi_{GL}(0)} + 0.12 \right) \quad (5)$$

Given $H_{c1}(0) = 2.85(3)$ mT, we determine $\lambda_{GL}(0) = 4909(8)$ Å. The resulting GL parameter defined as $k_{GL} = \frac{\lambda_{GL}(0)}{\xi_{GL}(0)}$, is found to be $k_{GL} = 57.4(4)$, which is significantly greater than $\frac{1}{\sqrt{2}}$, classifying NbTaOs₂ as a strong type-II superconductor. Furthermore, the thermodynamic critical field, $H_c(0)$, can be estimated using the relation $H_{c1}(0)H_{c2}(0) = H_c^2(0)\ln(k_{GL})$. The estimated value of $H_c(0)$ was found to be 56.3(2) mT for NbTaOs₂. The Maki parameter [57] is defined as the measure of the relative strength of the orbital and Pauli limiting effects in a superconductor. It is defined as $\alpha_M = \sqrt{2} \frac{H_{c2}^{orb}}{H^{Pauli}}$. Substituting the calculated values, we obtain $\alpha_M = 0.47(2)$, indicating that the paramagnetic effect on pair breaking is negligible.

It is essential to assess the stability of the vortex system against various factors that may disturb its equilibrium. The Ginzburg-Levanyuk number (G_i) quantifies the influence of thermal fluctuations on the process of vortex unpinning in a type-II superconductor [58] and is represented by Eq. (6).

$$G_i = \frac{1}{2} \left(\frac{k_B \mu_0 \tau T_c}{4\pi\xi(0)^3 H_c^2(0)} \right)^2 \quad (6)$$

Here, τ is the anisotropy factor (1 for cubic NbTaOs₂). We obtained $G_i = 1.45(4) \times 10^{-8}$ using the estimated parameters $T_c = 2.4(5)$ K, $\xi(0) = 85.4(4)$ Å and $H_c(0) = 56.3(2)$ mT. This value is close to low T_c superconductors ($\sim 10^{-8}$), suggesting that thermal fluctuations are not significantly responsible for the vortex unpinning in our compound [59].

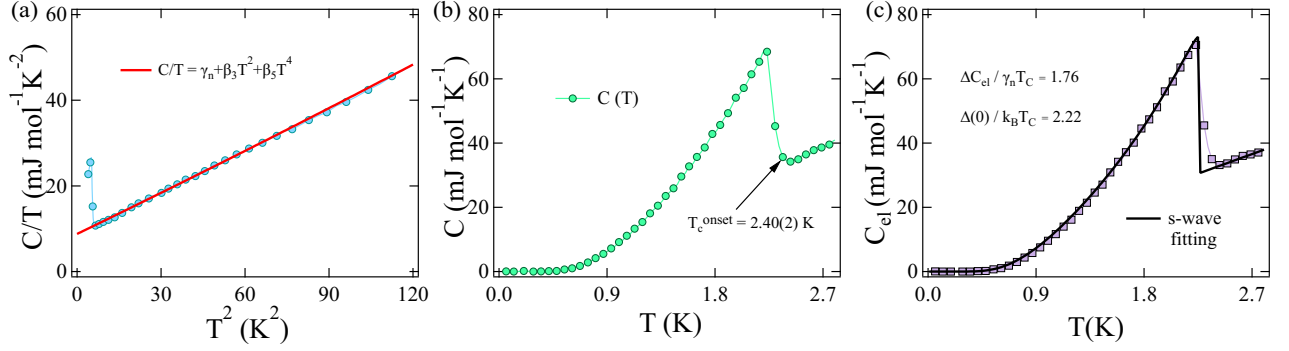


FIG. 3. (a) C/T vs. T^2 plot, where the solid red line represents a fit to Eq. (7) (b) Total specific heat vs. temperature plot (c) Temperature-dependent electronic-specific heat data, fitted by the isotropic single gap model, and the solid black curve shows the s-wave fitting.

D. Specific Heat

To further investigate the superconducting and normal state properties of NbTaOs₂, we performed a temperature-dependent specific heat $C(T)$ measurement. A distinct jump in specific heat was observed at $T_c = 2.40(2)$ K, as shown in Fig. 3 (b), consistent with the onset of diamagnetic signal in magnetization measurements. The specific heat data plotted as C/T vs T^2 in Fig. 3(a), analyzed using the Debye-Sommerfeld relation (Eq. (7))

$$C/T = \gamma_n + \beta_3 T^2 + \beta_5 T^4 \quad (7)$$

where γ_n is the Sommerfeld coefficient (electronic contribution to specific heat), β_3 corresponds to the phononic contribution, and β_5 captures the higher-order anharmonic effects. The best fit of Eq. (7) to the specific heat data in the normal state, shown as the red curve in Fig. 3(a), gives the parameters: $\gamma_n = 8.78(1)$ mJ mol⁻¹K⁻², $\beta_3 = 0.316(4)$ mJ mol⁻¹K⁻⁴ and $\beta_5 = 0.108(3)$ mJ mol⁻¹K⁻⁶.

γ_n is related to the density of states at the Fermi surface, $D(E_F)$, through the following relation;

$$\gamma_n = \left(\frac{\pi^2 k_B^2}{3} \right) D(E_F), \quad (8)$$

where k_B is the Boltzmann constant ($\simeq 1.38 \times 10^{-23}$ J K⁻¹). Using this relation, the density of states at the Fermi level for NbTaOs₂ is estimated to be $D(E_F) = 3.73(3)$ states/eV f.u. Furthermore, the Debye temperature (θ_{Debye}) can be estimated from the phononic coefficient β_3 using the Debye model,

$$\theta_{Debye} = \left(\frac{12\pi^4 RN}{5\beta_3} \right)^{\frac{1}{3}}, \quad (9)$$

where N represents the number of atoms per formula unit and $R = 8.314$ J mol⁻¹ K⁻¹ is the molar gas constant. Applying this formula, the Debye temperature for NbTaOs₂ is determined to be $\theta_{Debye} = 290(1)$ K.

The electron-phonon coupling strength can be evaluated using the dimensionless parameter λ_{e-ph} , derived from McMillan's model [60]. This parameter is calculated using estimated values of θ_{Debye} and T_c and is given by

$$\lambda_{e-ph} = \frac{1.04 + \mu \ln(\theta_{Debye}/1.45T_c)}{(1 - 0.62\mu) \ln(\theta_{Debye}/1.45T_c) - 1.04} \quad (10)$$

Here, μ represents the screened Coulomb repulsion, with a typical value of $\mu = 0.13$ used for transition metals [60]. Using $\theta_{Debye} = 290(1)$ K and $T_c = 2.25(3)$ K, the calculated electron-phonon coupling constant is $\lambda_{e-ph} = 0.53(4)$ [61, 62].

Figure 3(c) presents the temperature dependence of the electronic specific heat for NbTaOs₂. The electronic specific heat, C_{el} , is obtained by subtracting the phononic contribution, $C_{ph} = \beta_3 T^3 - \beta_5 T^5$, from the total specific heat, C . The magnitude of the electronic specific heat jump in the superconducting transition, characterized by $\frac{\Delta C_{el}}{\gamma_n T_c}$, is found to be 1.76(3). This value exceeds the prediction value (1.43) of the BCS theory in the weak-coupling limit, indicating moderate electron-phonon coupling in NbTaOs₂.

The symmetry of the superconducting gap can be examined by analyzing the temperature-dependent C_{el} . The relationship between normalized entropy (S) in the superconducting state and C_{el} is expressed as:

$$C_{el} = t \frac{dS}{dt}, \quad \text{where } t = T/T_c \quad (11)$$

Within the BCS framework, the normalized entropy for a single isotropic gap is given by

$$\frac{S}{\gamma_n T_c} = -\frac{6}{\pi^2} \left(\frac{\Delta(0)}{k_B T_c} \right) \int_0^\infty [f \ln(f) + (1-f) \ln(1-f)] dy, \quad (12)$$

where $f = [\exp(E(\xi)/k_B T) + 1]^{-1}$ is the Fermi function, and $E(\xi) = \sqrt{\xi^2 + \Delta^2(t)}$. Here, ξ represents the measured energy of normal electrons relative to the Fermi energy, and $y = \xi/\Delta(0)$.

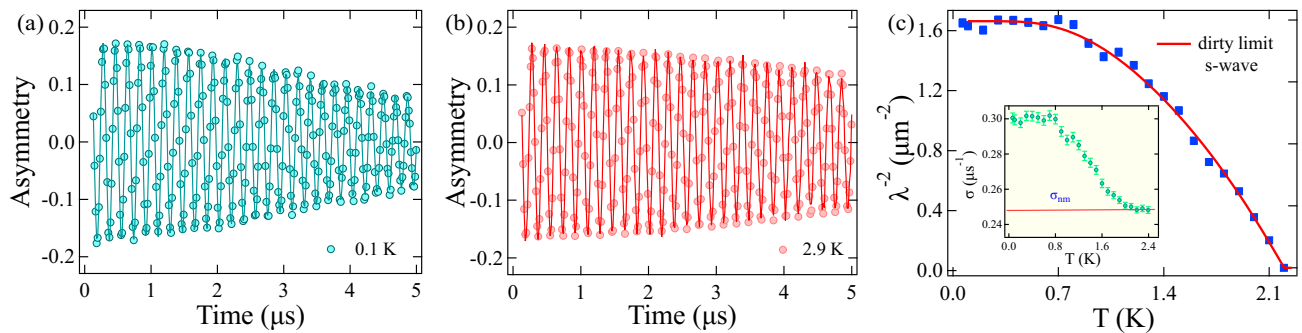


FIG. 4. TF- μ SR spectra collected (a) below (0.1 K) and (b) above (2.9 K) T_c . (c) Temperature dependence of inverse square penetration depth (λ^{-2}), where the red solid curve shows the dirty-limit s-wave fitting.

The temperature dependence of the superconducting gap in the BCS approximation is described by

$$\Delta(t) = \tanh[1.82(1.018((1/t) - 1))^{0.51}]. \quad (13)$$

The solid black curve in Fig. 3(c) represents the fit to the electronic specific heat data based on a single isotropic nodeless gap within the BCS model [63, 64]. It provides $\Delta(0)/k_B T_c = 2.22(1)$, which is higher than the standard BCS value of 1.76, indicating moderate electron-phonon coupling in NbTaOs₂.

E. Muon spin rotation and relaxation measurements

Transverse-field μ SR: We have performed μ SR measurements in the transverse field (TF) geometry to investigate the nature of the superconducting gap. In the normal state, a magnetic field of 40 mT was applied perpendicular to the initial muon spin direction, ensuring that it was above H_{c1} before cooling the sample to a base temperature of 0.1 K. The asymmetry spectra were recorded at different temperatures and the representative spectra measured below and above T_c are shown in Fig. 4(a) and (b), respectively. Furthermore, the time-domain spectra are accurately modeled using an oscillatory function combined with a Gaussian relaxation component as follows

$$A_{\text{TF}}(t) = \sum_{i=1}^N A_i \exp\left(\frac{-\sigma_i^2 t^2}{2}\right) \cos(\omega_i t + \phi) \quad (14)$$

where A_i is the initial asymmetry, σ_i is the depolarization rate, ϕ is the initial phase and ω_i is the precession frequency. Eq. (14) is used to fit the asymmetry spectra at different temperatures for $N = 2$, where σ_1 corresponds to muons interacting with the internal field distribution in the sample, while $\sigma_2 = 0$ corresponds to the background (silver sample holder).

The total depolarization rate (σ) is defined as

$$\sigma^2 = \sigma_{\text{fl}}^2 + \sigma_{\text{nm}}^2 \quad (15)$$

where σ_{fl} accounts for the contribution from FLL in the superconducting state, while σ_{nm} corresponds to the

relaxation due to randomly oriented nuclear dipole moments, which remains constant above T_c . The clear difference in σ between the $T < T_c$ spectra and those recorded in the normal state (as illustrated in Fig. 4(c)) is a direct consequence of the inhomogeneous field distribution induced by the FLL. In contrast, the weak Gaussian damping observed in the $T > T_c$ spectra arises from relaxation caused by randomly oriented nuclear dipolar fields [38, 46]. The inset of Fig. 4(c) shows the temperature dependence of σ for NbTaOs₂ measured at 40 mT. The nuclear contribution to the depolarization rate, $\sigma_{\text{nm}} = 0.2454(3) \mu\text{s}^{-1}$, is determined as the average depolarization rate above T_c . The superconducting contribution can then be extracted using Eq. (15). Furthermore, a well-ordered triangular or hexagonal Abrikosov vortex lattice is expected to form in the mixed state. The temperature-dependent magnetic penetration depth $\lambda(T)$ can be constructed from $\sigma_{\text{fl}}(T)$, using the simplified Brandt formula [65] under the primary condition that $H/H_{c2} \gg 1$.

$$\sigma_{\text{fl}}(T) = \frac{0.0609 \times \gamma_{\mu} \phi_0}{\lambda^2(T)} \quad (16)$$

where, ϕ_0 is defined as the magnetic flux quantum and $\gamma_{\mu} = 2\pi \times 135.5$ MHz/T is the muon gyromagnetic ratio. The temperature dependence of λ^{-2} , obtained from Eq. (16), is shown in Fig. 4(c). To analyze the temperature-dependent behavior of λ^{-2} , we employ the following function within London's approximation for a dirty-limit BCS superconductor [66]

$$\frac{\sigma_{\text{fl}}^{-2}(T)}{\sigma_{\text{fl}}^{-2}(0)} = \frac{\lambda^{-2}(T)}{\lambda^{-2}(0)} = \frac{\Delta(T)}{\Delta(0)} \tanh\left[\frac{\Delta(T)}{2k_B T}\right] \quad (17)$$

The temperature dependence of the energy gap in the BCS approximation is given by

$$\frac{\Delta(T)}{\Delta(0)} = \tanh[1.82(1.018((T_c/T) - 1))^{0.51}] \quad (18)$$

where $\Delta(0)$ represents the energy gap value at 0 K.

The solid red curve in Fig. 4(c) represents the fit obtained using Eq. (17), yielding $\Delta(0) = 0.38(2)$ meV

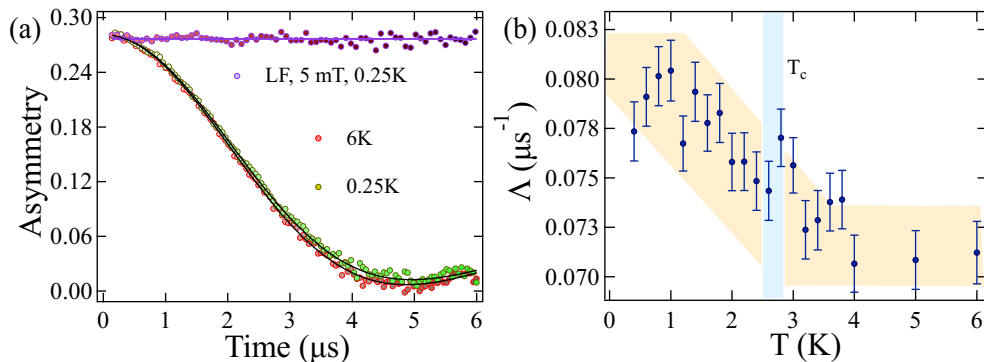


FIG. 5. (a) ZF- μ SR spectra collected below (0.25 K) and above (6 K) T_c and fitted using the static Kubo-Toyabe function with additional function as in Eq. (19). (b) Temperature-dependence of additional relaxation rate Λ with notable increase below T_c .

at 40 mT. This results in a normalized superconducting gap value of $\Delta(0)/k_B T_c = 2.02(1)$, which closely matches the value determined from our specific heat measurements. Additionally, the magnetic penetration depth at 0 K is estimated as $\lambda(0) = 7321(2)$ Å at 40 mT using Eq. (16). This value is slightly higher than the $\lambda(0)$ estimated from the magnetization measurements; this difference arises from the different methods used to determine the depth of penetration [67]. TF- μ SR and specific heat measurements indicate a fully open nodeless superconducting gap attributed to moderate electron-phonon coupling in NbTaOs₂.

Zero-field μ SR: Zero-field (ZF) μ SR measurements were performed to investigate the presence of spontaneous magnetic fields in the superconducting state of NbTaOs₂. Relaxation spectra were recorded in the absence of an external magnetic field. The ZF- μ SR spectra collected above ($T = 6$ K) and below ($T = 0.25$ K) T_c are presented in Fig. 5(a). To analyze the ZF- μ SR data at various temperatures, we use the fitting function given in Eq. (19). This function consists of a static Gaussian-type Kubo-Toyabe (KT) relaxation term ($G_{KT}(t)$) combined with an additional relaxation component and a constant background. The solid black curves in Fig. 5(a) represent the fits to the data using Eq. (19).

$$A(t) = A_i G_{KT}(t)e^{(-\Lambda t)^\beta} + A_{bg} \quad (19)$$

The KT function $G_{KT}(t)$, describes the asymmetry spectra associated with static and randomly oriented nuclear moments [68] and is given by

$$G_{KT}(t) = \frac{1}{3} + \frac{2}{3}(1 - \Delta_Z^2 t^2) \exp\left(\frac{-\Delta_Z^2 t^2}{2}\right) \quad (20)$$

Here, Δ_Z represents the relaxation rate due to nuclear dipolar fields, while A_i denotes the initial asymmetry. The temperature-independent background asymmetry, A_{bg} , originates from muons stopping in the silver sample holder. Λ corresponds to the additional relaxation rate, modified by a factor β . Across all temperature fits, β remained approximately 2 during the fitting [69].

As shown in Fig. 5(a), a subtle difference in the spectra above and below T_c suggests enhanced relaxation of the muon spin polarization in the superconducting state. Notably, when the KT relaxation rate, Δ_Z , A_i and A_{bg} remained fixed, the additional Gaussian relaxation rate, Λ , (for $\beta = 2$) exhibits a significant increase below T_c (see Fig. 5(b)), indicating the emergence of a weak spontaneous magnetic field. This relaxation rate remains nearly constant above T_c .

Further, longitudinal field (LF)- μ SR measurements were conducted to rule out the possibility that the observed increase in relaxation originates from dilute impurities. Applying a 5 mT field parallel to the muon spin direction at 0.25 K effectively decoupled the muon spin polarization from internal magnetic fields, as indicated by the nearly flat spectra (purple) in Fig. 5(a). This confirms that the relaxation observed in ZF- μ SR primarily arises from static internal fields. Additionally, the absence of oscillatory components in the LF spectra confirms the absence of magnetic ordering in our sample.

The magnitude of the internal magnetic field emerging below T_c was estimated using the relation [31]

$$B_{int} = \frac{\delta\Lambda}{\gamma_\mu} \quad (21)$$

where $\delta\Lambda$ represents the increase in the additional relaxation rate (Λ) observed below T_c , with parameters Δ_Z and β held constant. This increase was determined to be $0.008(1)$ μs^{-1} , yielding an internal field of $B_{int} = 0.094(5)$ G, and it is consistent with the values reported for NCS exhibiting TRSB [31, 33].

Our observation establishes NbTaOs₂ as the first member of the Re-free α -Mn cubic non-centrosymmetric (NC) structural family to exhibit time-reversal symmetry breaking (TRSB), given that previous μ SR investigations have not detected TRSB in other Re-free α -Mn NC superconductors [37–39, 42]. This finding challenges the assumption that Re is crucial for inducing TRSB in Re-based α -Mn superconductors like Re₆X (where X = Ti, Zr, Hf), where TRSB is commonly observed. The weak spontaneous magnetic field in NbTaOs₂ could be due to enhanced antisymmetric spin-orbit coupling (ASOC), possibly arising from the mixed 4d/5d sites within the

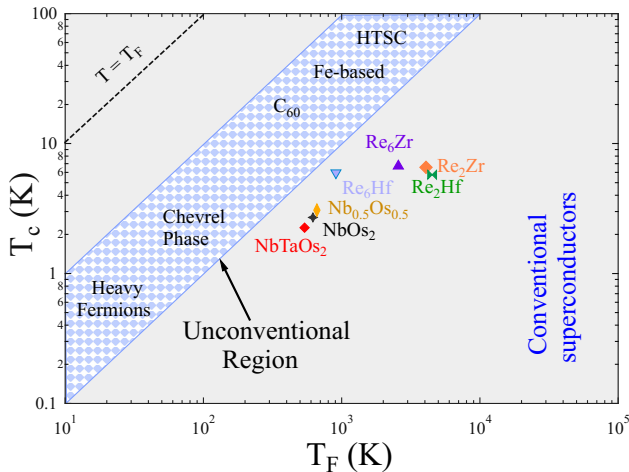


FIG. 6. T_c vs. T_F plot for Uemura classification where the red diamond represents NbTaOs_2 .

material. Although mixed sites can introduce disorder, a comparable residual resistivity ratio (RRR) in NbTaOs_2 to other NC binary superconductors suggests that TRSB in NbTaOs_2 is not driven by disorder, as recently proposed by Andersen et al. [70]. However, a complete understanding of the roles of SOC, site mixing, and intrinsic disorder in the α -Mn crystal structure requires further microscopic characterization of NbTaOs_2 samples with varying degrees of disorder, along with detailed electronic structure calculations.

IV. UEMURA PLOT

Uemura et al. [71] proposed a classification for superconductors based on the ratio of their superconducting transition temperature (T_c) to the Fermi temperature (T_F). Unconventional superconductors have ratios between $0.01 \leq T_c/T_F \leq 0.1$, distinguishing them from conventional superconductors, which have a significantly lower ratio. The Fermi temperature can be estimated using the expression $k_B T_F = \frac{\hbar^2}{2m_e} (3\pi^2 n_s)^{2/3} \frac{1}{(1+\lambda_{e-ph})}$, where k_B is the Boltzmann constant, \hbar is the reduced Planck constant, m_e is the electron mass, n_s is the density of super-electrons, and λ_{e-ph} represents the electron-phonon coupling constant. The density of super-electrons is related to the magnetic penetration depth (λ) and is given by [38]

$$n_s = \frac{m_e(1 + \lambda_{e-ph})}{\mu_0 e^2 \lambda^2} \quad (22)$$

Using λ_{e-ph} estimated from specific heat and λ calculated from muon analysis in Eq. (22) yields $n_s = 0.74(2) \times 10^{26} \text{ m}^{-3}$.

Using the evaluated value of n_s from Eq. (22) in the above expression for T_F , yielding $T_F = 539.5(2)$ K, further provides the ratio $T_c/T_F = 0.0044$, which places NbTaOs_2 just outside the unconventional region, as shown

TABLE I. Superconducting and normal state parameters of NbTaOs_2

Parameters	Unit	NbTaOs_2
T_c	K	2.4(2)
$H_{c1}(0)$	mT	2.85(3)
$H_{c2}(0)$	T	4.5(1)
$H_{c2}(0)^P$	T	4.46(2)
$H_{c2}(0)^{orb}(\text{T})$	T	1.5(1)
$\Delta C_{el}/\gamma_n T_C$		1.76(3)
$\Delta(0)/k_B T_C$		2.22(1)
γ_n	$\text{mJ mol}^{-1} \text{K}^{-2}$	8.78(1)
θ_D	K	290(1)
λ_{e-ph}		0.53(4)
$\xi_{GL}(0)$	\AA	85.4(4)
$\lambda_{GL}(0)$	\AA	4909(8)
k_{GL}		57.4(4)
$\lambda^{muon}(0)$	\AA	7321(2)
n_s	10^{26} m^{-3}	0.74(2)
T_F	K	539.5(2)

by the red diamond in Fig. 6. All superconducting and normal state parameters of NbTaOs_2 obtained from different techniques are listed in Table I.

V. CONCLUSION

In summary, we have successfully synthesized the Re-free ternary NbTaOs_2 with an α -Mn structure. Our comprehensive measurements, such as electrical resistivity, magnetization, and specific heat, confirm that it exhibits type-II bulk superconductivity. Electronic specific heat and transverse field μSR data point to a moderately coupled s-wave superconducting gap structure. Intriguingly, the zero-field μSR measurements indicate time-reversal symmetry breaking (TRSB) in the superconducting ground state of NbTaOs_2 . This marks the first observation of TRSB in a Re-free α -Mn compound, which we believe is due to the enhanced spin-orbit coupling resulting from 4d/5d side mixing. This study not only paves the way for inducing TRSB in superconducting ground states but also offers further insights into the role of disorder in superconductivity, a topic that remains poorly understood.

VI. ACKNOWLEDGEMENT

R.K.K. thanks the UGC, Government of India, for a Senior Research Fellowship. R.P.S. acknowledges the SERB Government of India (Core Research Grant CRG/2023/000817). We also thank ISIS, STFC, UK, for μSR beamtime (RB: 2410330).

- [1] M. Sigrist and K. Ueda, Phenomenological theory of unconventional superconductivity, *Rev. Mod. Phys.* **63**, 239 (1991).
- [2] E. Bauer, G. Hilscher, H. Michor, C. Paul, E. W. Scheidt, A. Griбанov, Y. Seropegin, H. Noël, M. Sigrist, and P. Rogl, Heavy fermion superconductivity and magnetic order in noncentrosymmetric CePt₃Si, *Phys. Rev. Lett.* **92**, 027003 (2004).
- [3] M. Smidman, M. B. Salamon, H. Q. Yuan, and D. F. Agterberg, Superconductivity and spin-orbit coupling in non-centrosymmetric materials: a review, *Rep. Prog. Phys.* **80**, 036501 (2017).
- [4] L. P. Gor'kov and E. I. Rashba, Superconducting 2d system with lifted spin degeneracy: Mixed singlet-triplet state, *Phys. Rev. Lett.* **87**, 037004 (2001).
- [5] H. Takeya, M. ElMassalami, S. Kasahara, and K. Hirata, Specific-heat studies of the spin-orbit interaction in noncentrosymmetric Li₂Pd_{1-x}Pt_xB ($x = 0, 0.5, 1$) superconductors, *Phys. Rev. B* **76**, 104506 (2007).
- [6] J. Chen, M. B. Salamon, S. Akutagawa, J. Akimitsu, J. Singleton, J. L. Zhang, L. Jiao, and H. Q. Yuan, Evidence of nodal gap structure in the noncentrosymmetric superconductor Y₂C₃, *Phys. Rev. B* **83**, 144529 (2011).
- [7] S. Kuroiwa, Y. Saura, J. Akimitsu, M. Hiraishi, M. Miyazaki, K. H. Satoh, S. Takeshita, and R. Kadono, Multigap superconductivity in sesquicarbides La₂C₃ and Y₂C₃, *Phys. Rev. Lett.* **100**, 097002 (2008).
- [8] A. B. Karki, Y. M. Xiong, I. Vekhter, D. Browne, P. W. Adams, D. P. Young, K. R. Thomas, J. Y. Chan, H. Kim, and R. Prozorov, Structure and physical properties of the noncentrosymmetric superconductor Mo₃Al₂C, *Phys. Rev. B* **82**, 064512 (2010).
- [9] A. P. Schnyder and S. Ryu, Topological phases and surface flat bands in superconductors without inversion symmetry, *Phys. Rev. B* **84**, 060504 (2011).
- [10] A. P. Schnyder, P. M. R. Brydon, and C. Timm, Types of topological surface states in nodal noncentrosymmetric superconductors, *Phys. Rev. B* **85**, 024522 (2012).
- [11] K. P. Sajilesh, R. K. Kushwaha, D. Samanta, T. Tula, P. K. Meena, S. Srivastava, D. Singh, P. K. Biswas, A. Kanigel, A. D. Hillier, S. K. Ghosh, and R. P. Singh, Time-reversal symmetry breaking superconductivity in HfRhGe: A noncentrosymmetric weyl semimetal, *Adv. Mat.* **36**, 2415721 (2024).
- [12] A. Kapustin and L. Radzihovsky, Piezosuperconductivity: Novel effects in noncentrosymmetric superconductors, *Phys. Rev. B* **105**, 134514 (2022).
- [13] P. K. Biswas, H. Luetkens, T. Neupert, T. Stürzer, C. Baines, G. Pascua, A. P. Schnyder, M. H. Fischer, J. Goryo, M. R. Lees, H. Maeter, F. Brückner, H.-H. Klauss, M. Nicklas, P. J. Baker, A. D. Hillier, M. Sigrist, A. Amato, and D. Johrendt, Evidence for superconductivity with broken time-reversal symmetry in locally noncentrosymmetric SrPtAs, *Phys. Rev. B* **87**, 180503 (2013).
- [14] J. Garaud, M. N. Chernodub, and D. E. Kharzeev, Vortices with magnetic field inversion in noncentrosymmetric superconductors, *Phys. Rev. B* **102**, 184516 (2020).
- [15] H. Tanaka, H. Watanabe, and Y. Yanase, Nonlinear optical responses in noncentrosymmetric superconductors, *Phys. Rev. B* **107**, 024513 (2023).
- [16] G. Tkachov, Probing the magnetoelectric effect in non-centrosymmetric superconductors by equal-spin andreev tunneling, *Journal of Physics: Condensed Matter* **31**, 055301 (2018).
- [17] J. Garaud, A. Korneev, A. Samoilenka, A. Molochkov, E. Babaev, and M. Chernodub, Counterpart of the chandrasekhar-kendall state in noncentrosymmetric superconductors, *Phys. Rev. B* **108**, 014504 (2023).
- [18] M. Nadeem, M. S. Fuhrer, and X. Wang, The superconducting diode effect, *Nat. Rev. Phys.* **5**, 558 (2023).
- [19] A. Daido, Y. Ikeda, and Y. Yanase, Intrinsic superconducting diode effect, *Phys. Rev. Lett.* **128**, 037001 (2022).
- [20] H. Narita, J. Ishizuka, R. Kawarazaki, D. Kan, Y. Shiota, T. Moriyama, Y. Shimakawa, A. V. Ognev, A. S. Samardak, Y. Yanase, *et al.*, Field-free superconducting diode effect in noncentrosymmetric superconductor/ferromagnet multilayers, *Nat. Nanotechnol.* **17**, 823 (2022).
- [21] H. Narita, J. Ishizuka, D. Kan, Y. Shimakawa, Y. Yanase, and T. Ono, Magnetization control of zero-field intrinsic superconducting diode effect, *Adv. Mat.* **35**, 2304083 (2023).
- [22] S. K. Ghosh, M. Smidman, T. Shang, J. F. Annett, A. D. Hillier, J. Quintanilla, and H. Yuan, Recent progress on superconductors with time-reversal symmetry breaking, *J. Phys.: Condens. Matter* **33**, 033001 (2020).
- [23] H. Deng, G. Liu, Z. Guguchia, T. Yang, J. Liu, Z. Wang, Y. Xie, S. Shao, H. Ma, W. Liège, *et al.*, Evidence for time-reversal symmetry-breaking kagome superconductivity, *Nat. Mat.* , 1 (2024).
- [24] W.-C. Lee, S.-C. Zhang, and C. Wu, Pairing state with a time-reversal symmetry breaking in FeAs-based superconductors, *Phys. Rev. Lett.* **102**, 217002 (2009).
- [25] J. Xia, Y. Maeno, P. T. Beyersdorf, M. M. Fejer, and A. Kapitulnik, High resolution polar kerr effect measurements of Sr₂RuO₄: Evidence for broken time-reversal symmetry in the superconducting state, *Phys. Rev. Lett.* **97**, 167002 (2006).
- [26] G. M. Luke, Y. Fudamoto, K. M. Kojima, M. I. Larkin, J. Merrin, B. Nachumi, Y. J. Uemura, Y. Maeno, Z. Q. Mao, Y. Mori, and M. Nakamura, H. and Sigrist, Time-reversal symmetry-breaking superconductivity in Sr₂RuO₄, *Nature (London)* **394**, 558 (1998).
- [27] H. Weber, D. Weitbrecht, D. Brach, A. Shelankov, H. Keiter, W. Weber, T. Wolf, J. Geerk, G. Linker, G. Roth, P. Splittgerber-Hünnekes, and G. Güntherodt, Evidence for broken time reversal symmetry in cuprate superconductors, *Solid State Commun.* **76**, 511 (1990).
- [28] M. Oudah, Y. Cai, M. V. D. T. Sanchez, J. Bannies, M. C. Aronson, K. M. Kojima, and D. A. Bonn, Time-reversal symmetry breaking superconductivity in CaSb₂, *Phys. Rev. B* **110**, 134524 (2024).
- [29] R. P. Singh, A. D. Hillier, B. Mazidian, J. Quintanilla, J. F. Annett, D. M. Paul, G. Balakrishnan, and M. R. Lees, Detection of time-reversal symmetry breaking in the noncentrosymmetric superconductor Re₆Zr using muon-spin spectroscopy, *Phys. Rev. Lett.* **112**, 107002 (2014).
- [30] D. Singh, J. A. T. Barker, A. Thamizhavel, D. M. Paul, A. D. Hillier, and R. P. Singh, Time-reversal symmetry breaking in the noncentrosymmetric superconductor Re₆Hf: Further evidence for unconventional behavior in

- the α -Mn family of materials, *Phys. Rev. B* **96**, 180501 (2017).
- [31] D. Singh, K. P. Sajilesh, J. A. T. Barker, D. M. Paul, A. D. Hillier, and R. P. Singh, Time-reversal symmetry breaking in the noncentrosymmetric superconductor Re_6Ti , *Phys. Rev. B* **97**, 100505 (2018).
- [32] J. A. T. Barker, D. Singh, A. Thamizhavel, A. D. Hillier, M. R. Lees, G. Balakrishnan, D. M. Paul, and R. P. Singh, Unconventional superconductivity in La_7Ir_3 revealed by muon spin relaxation: Introducing a new family of noncentrosymmetric superconductor that breaks time-reversal symmetry, *Phys. Rev. Lett.* **115**, 267001 (2015).
- [33] D. Singh, M. S. Scheurer, A. D. Hillier, D. T. Adroja, and R. P. Singh, Time-reversal-symmetry breaking and unconventional pairing in the noncentrosymmetric superconductor La_7Rh_3 , *Phys. Rev. B* **102**, 134511 (2020).
- [34] Arushi, D. Singh, A. D. Hillier, M. S. Scheurer, and R. P. Singh, Time-reversal symmetry breaking and multigap superconductivity in the noncentrosymmetric superconductor La_7Ni_3 , *Phys. Rev. B* **103**, 174502 (2021).
- [35] M. O. Ajeesh, M. Bordelon, C. Girod, S. Mishra, F. Ronning, E. D. Bauer, B. Majorov, J. D. Thompson, P. F. S. Rosa, and S. M. Thomas, Fate of time-reversal symmetry breaking in UTe_2 , *Phys. Rev. X* **13**, 041019 (2023).
- [36] G. M. Luke, A. Keren, L. P. Le, W. D. Wu, Y. J. Uemura, D. A. Bonn, L. Taillefer, and J. D. Garrett, Muon spin relaxation in UPt_3 , *Phys. Rev. Lett.* **71**, 1466 (1993).
- [37] D. Singh, J. A. T. Barker, A. Thamizhavel, A. D. Hillier, D. M. Paul, and R. P. Singh, Superconducting properties and μSR study of the noncentrosymmetric superconductor $\text{Nb}_{0.5}\text{Os}_{0.5}$, *J. Phys.: Condens. Matter* **30**, 075601 (2018).
- [38] D. Singh, K. P. Sajilesh, S. Marik, A. D. Hillier, and R. P. Singh, Superconducting and normal state properties of the noncentrosymmetric superconductor NbOs_2 investigated by muon spin relaxation and rotation, *Phys. Rev. B* **99**, 014516 (2019).
- [39] D. Singh, K. P. Sajilesh, S. Marik, P. K. Biswas, A. D. Hillier, and R. P. Singh, Nodeless s-wave superconductivity in the α -Mn structure type noncentrosymmetric superconductor TaOs : a μSR study, *J. Phys.: Condens. Matter* **32**, 015602 (2019).
- [40] P. K. Biswas, A. D. Hillier, M. R. Lees, and D. M. Paul, Comparative study of the centrosymmetric and noncentrosymmetric superconducting phases of Re_3W using muon spin spectroscopy and heat capacity measurements, *Phys. Rev. B* **85**, 134505 (2012).
- [41] J. A. T. Barker, B. D. Breen, R. Hanson, A. D. Hillier, M. R. Lees, G. Balakrishnan, D. M. Paul, and R. P. Singh, Superconducting and normal-state properties of the noncentrosymmetric superconductor Re_3Ta , *Phys. Rev. B* **98**, 104506 (2018).
- [42] A. A. Aczel, T. J. Williams, T. Goko, J. P. Carlo, W. Yu, Y. J. Uemura, T. Klimczuk, J. D. Thompson, R. J. Cava, and G. M. Luke, Muon spin rotation/relaxation measurements of the noncentrosymmetric superconductor $\text{Mg}_{10}\text{Ir}_{19}\text{B}_{16}$, *Phys. Rev. B* **82**, 024520 (2010).
- [43] T. Shang, M. Smidman, S. K. Ghosh, C. Baines, L. J. Chang, D. J. Gawryluk, J. A. T. Barker, R. P. Singh, D. M. Paul, G. Balakrishnan, E. Pomjakushina, M. Shi, M. Medarde, A. D. Hillier, H. Q. Yuan, J. Quintanilla, J. Mesot, and T. Shiroka, Time-reversal symmetry breaking in Re-Based superconductors, *Phys. Rev. Lett.* **121**, 257002 (2018).
- [44] J. Rodríguez-Carvajal, Recent advances in magnetic structure determination by neutron powder diffraction, *Phys. B: Condens. Matter* **192**, 55 (1993).
- [45] A. D. Hillier, S. J. Blundell, I. McKenzie, I. Umegaki, L. Shu, J. A. Wright, T. Prokscha, F. Bert, K. Shimomura, A. Berlie, *et al.*, Muon spin spectroscopy, *Nat. Rev. Methods Primers* **2**, 4 (2022).
- [46] R. K. Kushwaha, Arushi, S. Sharma, S. Srivastava, P. K. Meena, M. Pula, J. Beare, J. Gautreau, A. D. Hillier, G. M. Luke, and R. P. Singh, Unconventional properties of the noncentrosymmetric superconductor Re_8NbTa , *Phys. Rev. B* **109**, 174518 (2024).
- [47] F. Han, C. D. Malliakas, C. C. Stoumpos, M. Sturza, H. Claus, D. Y. Chung, and M. G. Kanatzidis, Superconductivity and strong intrinsic defects in $\text{lapd}_{1-x}\text{bi}_2$, *Phys. Rev. B* **88**, 144511 (2013).
- [48] E. Helfand and N. R. Werthamer, Temperature and purity dependence of the superconducting critical field, H_{c2} . II, *Phys. Rev.* **147**, 288 (1966).
- [49] N. R. Werthamer, E. Helfand, and P. C. Hohenberg, Temperature and purity dependence of the superconducting critical field, H_{c2} . III. electron spin and spin-orbit effects, *Phys. Rev.* **147**, 295 (1966).
- [50] A. B. Karki, Y. M. Xiong, I. Vekhter, D. Browne, P. W. Adams, D. P. Young, K. R. Thomas, J. Y. Chan, H. Kim, and R. Prozorov, Structure and physical properties of the noncentrosymmetric superconductor $\text{Mo}_3\text{Al}_2\text{C}$, *Phys. Rev. B* **82**, 064512 (2010).
- [51] J.-K. Bao, J.-Y. Liu, C.-W. Ma, Z.-H. Meng, Z.-T. Tang, Y.-L. Sun, H.-F. Zhai, H. Jiang, H. Bai, C.-M. Feng, Z.-A. Xu, and G.-H. Cao, Superconductivity in quasi-one-dimensional $\text{K}_2\text{Cr}_3\text{As}_3$ with significant electron correlations, *Phys. Rev. X* **5**, 011013 (2015).
- [52] V. P. Mineev and K. V. Samokhin, Effects of impurities on superconductivity in noncentrosymmetric compounds, *Phys. Rev. B* **75**, 184529 (2007).
- [53] J. Lu, O. Zheliuk, I. Leermakers, N. F. Yuan, U. Zeitler, K. T. Law, and J. Ye, Evidence for two-dimensional ising superconductivity in gated MoS_2 , *Science* **350**, 1353 (2015).
- [54] X. Xi, Z. Wang, W. Zhao, J.-H. Park, K. T. Law, H. Berger, L. Forró, J. Shan, and K. F. Mak, Ising pairing in superconducting NbSe_2 atomic layers, *Nat. Phys.* **12**, 139 (2016).
- [55] M. Tinkham, *Introduction to superconductivity*, Vol. 1 (Courier Corporation, 2004).
- [56] T. Klimczuk, F. Ronning, V. Sidorov, R. J. Cava, and J. D. Thompson, Physical properties of the noncentrosymmetric superconductor $\text{Mg}_{10}\text{Ir}_{19}\text{B}_{16}$, *Phys. Rev. Lett.* **99**, 257004 (2007).
- [57] E. Ambler, J. H. Colwell, W. R. Hosler, and J. F. Schooley, Magnetization and critical fields of superconducting SrTiO_3 , *Phys. Rev.* **148**, 280 (1966).
- [58] O. Prakash, A. Thamizhavel, and S. Ramakrishnan, Multiband superconductivity in $\text{Lu}_3\text{Os}_4\text{Ge}_{13}$, *Supercond. Sci. Technol.* **28**, 115012 (2015).
- [59] A. E. Koshelev, K. Willa, R. Willa, M. P. Smylie, J.-K. Bao, D. Y. Chung, M. G. Kanatzidis, W.-K. Kwok, and U. Welp, Melting of vortex lattice in the magnetic superconductor $\text{RbEuFe}_4\text{As}_4$, *Phys. Rev. B* **100**, 094518 (2019).
- [60] W. L. McMillan, Transition temperature of strongly coupled superconductors, *Phys. Rev.* **167**, 331 (1968).
- [61] A. Bhattacharyya, D. Adroja, N. Kase, A. Hillier, J. Akimitsu, and A. Strydom, Unconventional supercon-

- ductivity in $\text{Y}_5\text{Rh}_6\text{Sn}_{18}$ probed by muon spin relaxation, *Sci. Rep.* **5**, 12926 (2015).
- [62] D. T. Adroja, A. Bhattacharyya, M. Telling, Y. Feng, M. Smidman, B. Pan, J. Zhao, A. D. Hillier, F. L. Pratt, and A. M. Strydom, Superconducting ground state of quasi-one-dimensional $\text{K}_2\text{Cr}_3\text{As}_3$ investigated using μSR measurements, *Phys. Rev. B* **92**, 134505 (2015).
- [63] J. Bardeen, L. N. Cooper, and J. R. Schrieffer, Theory of superconductivity, *Phys. Rev.* **108**, 1175 (1957).
- [64] H. Suhl and B. T. Matthias, Exchange scattering in superconductors, *Phys. Rev. Lett.* **2**, 5 (1959).
- [65] E. H. Brandt, Properties of the ideal ginzburg-landau vortex lattice, *Phys. Rev. B* **68**, 054506 (2003).
- [66] A. Carrington and F. Manzano, Magnetic penetration depth of MgB_2 , *Physica C* **385**, 205 (2003).
- [67] V. K. Anand, D. T. Adroja, M. R. Lees, P. K. Biswas, A. D. Hillier, and B. Lake, Superconductivity in $\text{Ru}_{0.55}\text{Rh}_{0.45}\text{P}$ and $\text{Ru}_{0.75}\text{Rh}_{0.25}\text{As}$ probed by muon spin relaxation and rotation measurements, *Phys. Rev. B* **98**, 214517 (2018).
- [68] R. S. Hayano, Y. J. Uemura, J. Imazato, N. Nishida, T. Yamazaki, and R. Kubo, Zero-and low-field spin relaxation studied by positive muons, *Phys. Rev. B* **20**, 850 (1979).
- [69] M. Fujihala, H. Koorikawa, S. Mitsuda, K. Morita, T. Tohyama, K. Tomiyasu, A. Koda, H. Okabe, S. Itoh, T. Yokoo, *et al.*, Possible tomonaga-luttinger spin liquid state in the spin-1/2 inequilateral diamond-chain compound $\text{K}_3\text{Cu}_3\text{AlO}_2(\text{SO}_4)_4$, *Sci. Rep.* **7**, 16785 (2017).
- [70] B. M. Andersen, A. Kreisel, and P. J. Hirschfeld, Spontaneous time-reversal symmetry breaking by disorder in superconductors, *Front. Phys.* **12** (2024).
- [71] Y. J. Uemura, V. J. Emery, A. R. Moodenbaugh, M. Suenaga, D. C. Johnston, A. J. Jacobson, J. T. Lewandowski, J. H. Brewer, R. F. Kiefl, S. R. Kreitzman, G. M. Luke, T. Riseman, C. E. Stronach, W. J. Kossler, J. R. Kempton, X. H. Yu, D. Opie, and H. E. Schone, Systematic variation of magnetic-field penetration depth in high- T_c superconductors studied by muon-spin relaxation, *Phys. Rev. B* **38**, 909 (1988).